



Division of Engineering
Brown University

Finite Element Analysis of the Concept Load Cell for the TerraTek Single Cutter Tester

EN175 Class of 1999, Inc.

A.F. Bower, Division of Engineering, Brown University, Providence RI 02912
Tel (401) 863 1493. Fax (401) 863 1157 Email Allan_Bower@brown.edu

Summary

This report describes a finite element analysis of the Concept Load Cell for the TerraTek Single Cutter Tester.

We have calculated calibration factors for the load cell, by computing strain distributions in the gage section for various combinations of loading. These computations show that:

- (a) Axial loading induces significant bending in the gage section of the load cell, causing a non-uniform strain distribution in the gage section of the load cell.
- (b) It is simplest to calibrate the load cell by averaging strain readings from gages mounted at two diametrically opposed points on the load cell wall. Calibration factors listed in Section 4 may then be used to determine forces acting on the load cell.
- (c) There is a small error in the load cell calibration due to contact between the inner section of the load cell and its casing. This error depends on the magnitude of the transverse load and the position of the tool, but will not exceed 5%.

We have also computed the stress distribution in the load cell at maximum specified load, and estimate a safety factor of approximately 1.3 against yield in the load cell gage section.

1. Problem Statement

The load cell is sketched in Fig. 1. The cell is to be loaded by an axial force F_A and transverse force F_T , which act on the tool as shown. The positions of the forces are specified by their height h below the base of the load cell, and the radial distance R from the axis of symmetry. Both h and R are variable.

Our objective is to compute the distribution of strain in the gage section of the load cell caused by arbitrary axial and transverse loading. In addition, we will compute a safety factor for the load cell under the maximum specified loading.

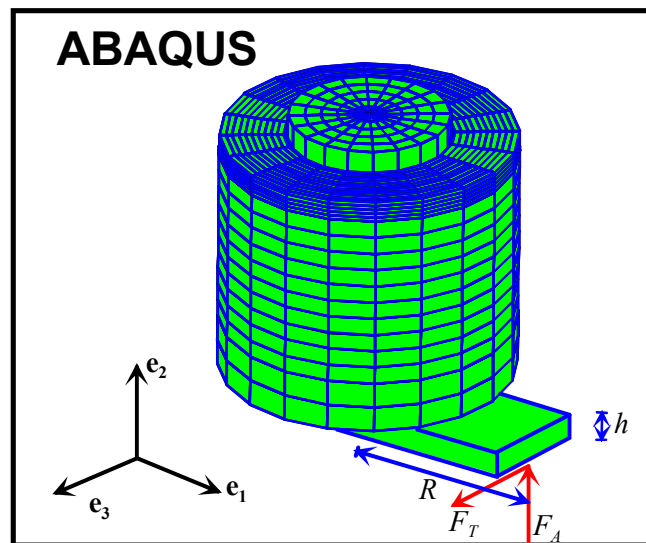


Fig. 1: 3D view of the TerraTek Concept Load Cell.

A cross section through our finite element model (showing the mesh used for some 3D computations) is shown in Fig. 2. The holder mount has not been modeled explicitly: instead, the forces acting on the load cell have been represented by a statically equivalent system of forces and moments acting on the base of the load cell on the axis of symmetry, as shown.

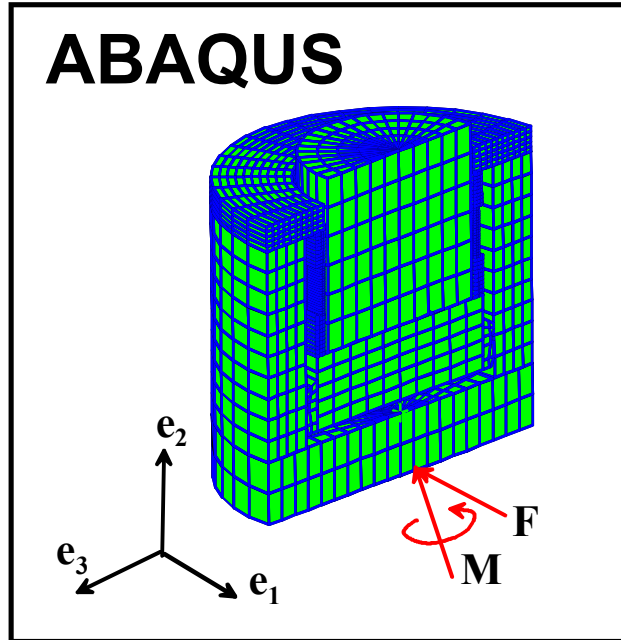


Fig. 2: The statically equivalent load system used in finite element computations.

An elementary calculation shows the statically equivalent forces and moments to be

$$\mathbf{F} = F_r \mathbf{e}_3 + F_A \mathbf{e}_2$$

$$\mathbf{M} = F_r h \mathbf{e}_1 - F_r R \mathbf{e}_2 + F_A R \mathbf{e}_3$$

The applied forces are halved in computations where symmetry conditions require only one half the load cell to be meshed.

We have conducted four sets of finite element computations to determine calibration factors for the load cell:

1. Unit axial loading parallel to the axis of revolution (axisymmetric)
2. Unit torsional loading parallel to the axis of revolution (generalized axisymmetry)
3. Unit force perpendicular to the axis of revolution (3D)
4. Unit moment perpendicular to the axis of revolution (3D)

This information may be used to determine the total distribution of strain in the load cell for arbitrary tool forces and with an arbitrary position of the tool.

We have also conducted one fully three dimensional computation under worst case loading to check the calibration and to estimate a safety factor for the load cell.

We have made the following assumptions in all FEM computations:

1. Material was idealized as an isotropic, linear elastic solid, with Young's Modulus 30×10^6 psi and Poisson's ratio 0.31;
2. All bolted joints were idealized as perfect bonds;
3. We have accounted for contact between the inner and outer sections of the load cell under transverse loading and moment. Except where noted, friction at this contact was neglected;

4. All parts were assumed to be manufactured exactly to specified dimensions.

All strains to be reported in the sections to follow will be expressed as components in a cylindrical—polar basis $\{\mathbf{e}_r, \mathbf{e}_\theta, \mathbf{e}_z\}$ shown in Fig. 8. Note further that the ‘mathematical’ definition of shear strain

$$\varepsilon_{z\theta} = \frac{1}{2} \left(\frac{1}{r} \frac{\partial u_z}{\partial \theta} + \frac{\partial u_\theta}{\partial z} \right)$$

is used throughout this report (this is one half the definition used in most elementary strength of materials texts).

2. Finite Element Simulations

2.1 Axial Loading

Fig. 3 shows the mesh and boundary conditions used to investigate the load cell behavior under purely axial loading.

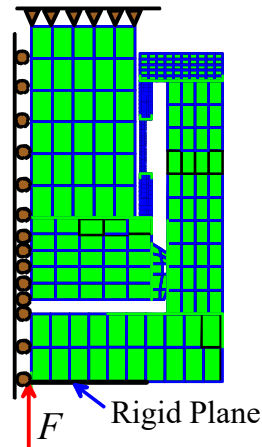


Fig. 3: The finite element mesh used for axial loading

Fig. 4 shows the deformation induced in the gage section of the load cell due to unit axial loading. The variations of axial strain ε_{zz} and hoop strain $\varepsilon_{\theta\theta}$ with distance from the gage section centerline are plotted in Fig 5. Results are shown for both the inner and outer surface of the gage section. The fluctuations in strain near the top and bottom of the gage section are spurious and caused by lack of mesh resolution in these regions.

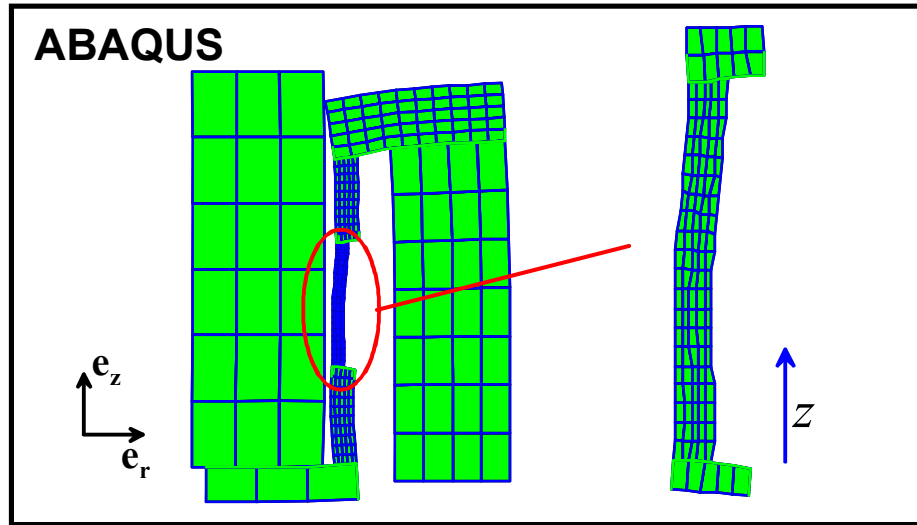


Fig. 4: Deformation induced in the load cell by axial loading. Displacements are magnified to show the deformation clearly.

For comparison, the strains induced in a cylinder with wall thickness 0.1in and radius 2in by axial loading are $\varepsilon_{zz} / F = 2.7206 \times 10^{-8} \text{ [lb}^{-1}\text{]}$ and $\varepsilon_{\theta\theta} / F = -8.434 \times 10^{-9} \text{ [lb}^{-1}\text{]}$.

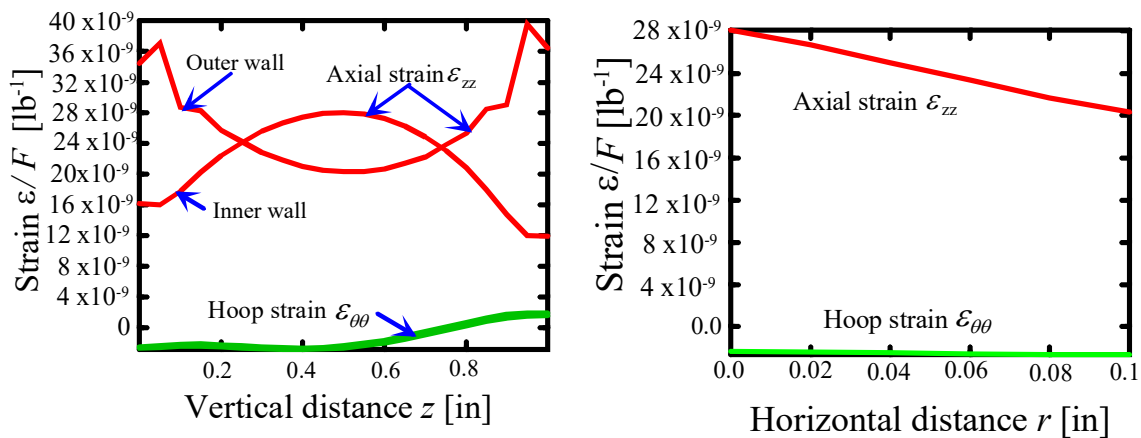


Fig. 5: Variation of strain in the load cell gage section due to axial loading.

Note that our simulations predict that significant bending will be induced in the gage section of the load cell by axial loading. This has several consequences:

- (1) The vertical strain ε_{zz} varies vertically up the gage section of the cell (Fig. 5)
- (2) The vertical strain ε_{zz} varies through the thickness of the gage section. (Fig 5)
- (3) Substantial hoop stresses $\sigma_{\theta\theta}$ are induced in the gage section. The hoop strain $\varepsilon_{\theta\theta}$ therefore differs from the expected value $\varepsilon_{\theta\theta} = -\nu\varepsilon_{zz}$

2.2 Torsional Loading

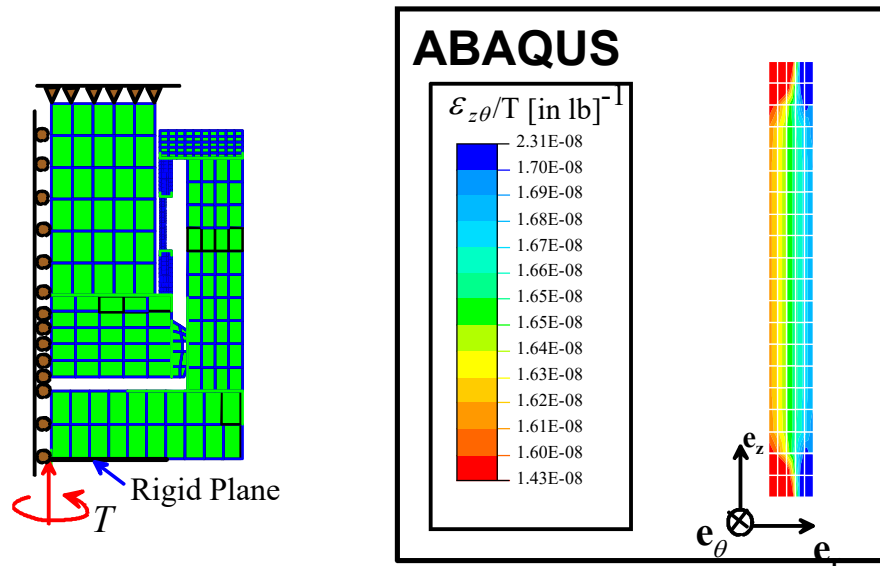


Fig. 6: Contours of strain in the load cell gage section due to torsional loading.

Fig. 6 shows contours of normalized shear strain $\varepsilon_{z\theta}/T$ induced in the gage section of the load cell by torsional loading parallel to the axis of revolution. There is negligible variation in shear strain in the region of interest near the center of the gage section. Our computations predict $\varepsilon_{z\theta}/T = 1.61 \times 10^{-8}$ [in lb] $^{-1}$ on the inner wall and $\varepsilon_{z\theta}/T = 1.69 \times 10^{-8}$ [in lb] $^{-1}$ on the outer wall of the gage section. This is identical to the result predicted by elementary strength of materials theory.

2.3 Loading by Transverse Force

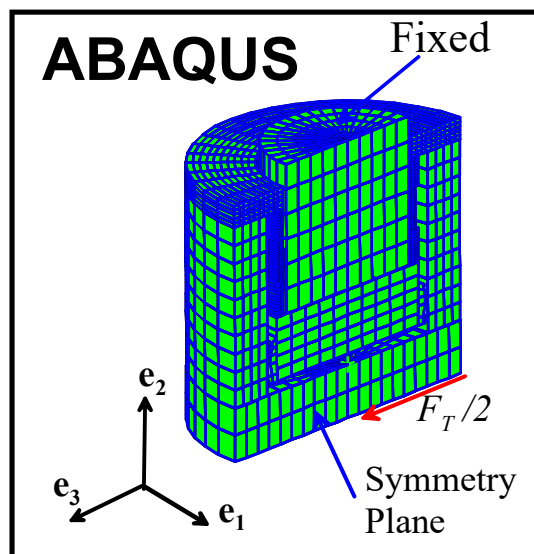
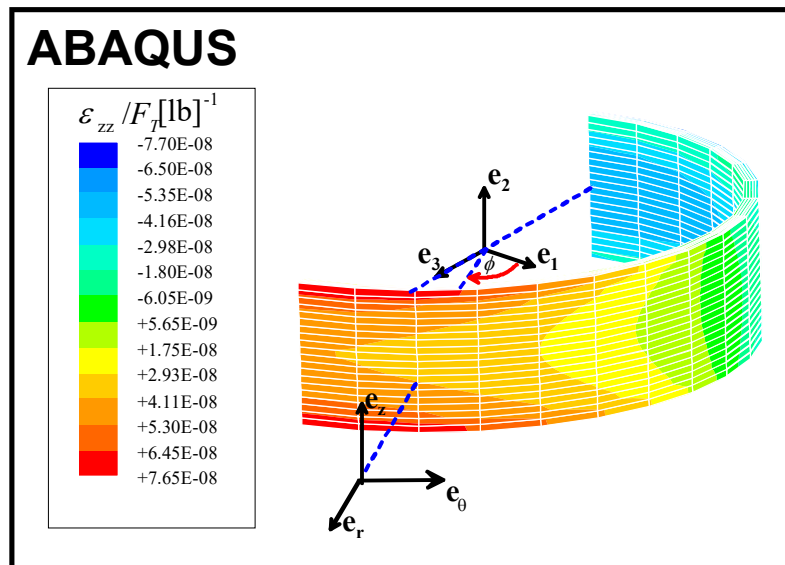
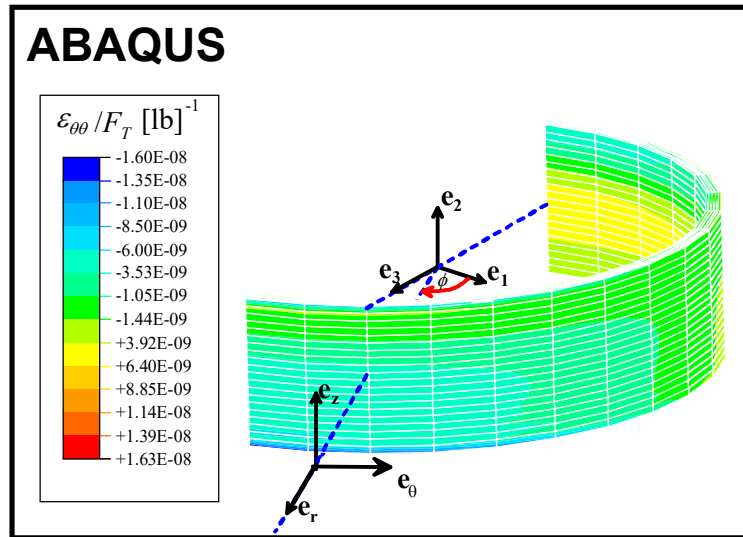


Fig. 7: Finite element mesh used to compute strains induced by transverse loading.

Fig. 8 shows contours of normalized axial strain ε_{zz} / F_T , hoop strain $\varepsilon_{\theta\theta} / F_T$ and shear strain $\varepsilon_{z\theta} / F_T$ induced in the gage section of the load cell by a transverse force applied to the base, as shown.



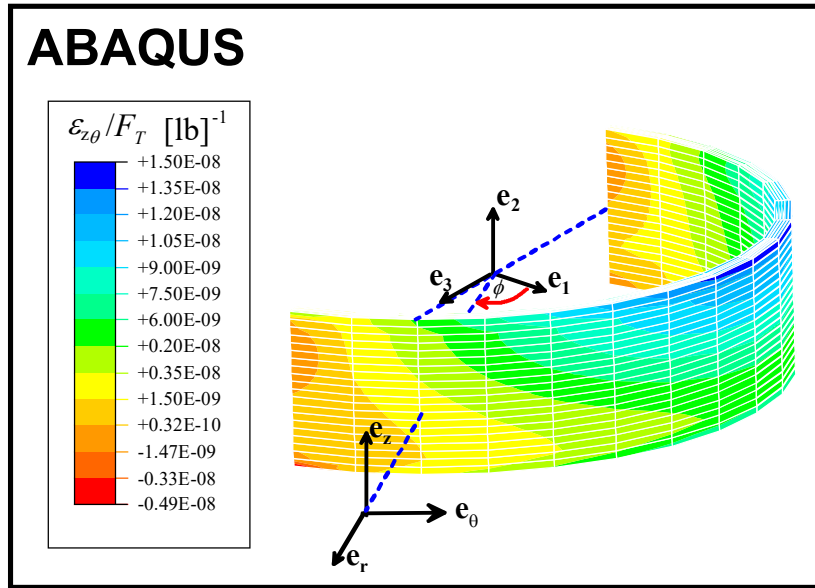


Fig. 8: Contours of strain induced in the gage section of the load cell by transverse loading.

The circumferential variation of each strain component at the midpoint of the gage section is plotted in Fig. 9. Results are shown for both the inner (solid line) and outer (dashed line) wall of the gage section. All strain values were computed for a transverse load $F_T = 15000\text{lb}$.

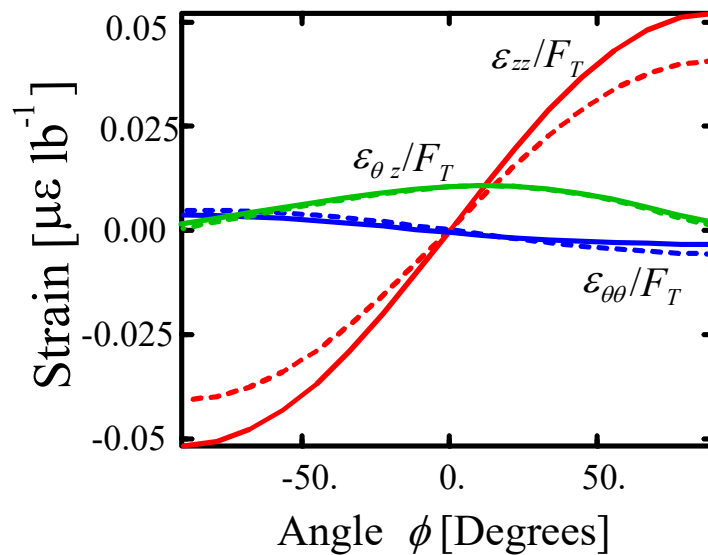


Fig. 9: Circumferential variation of strain at the mid section of the load cell due to transverse loading. The solid line shows strains on the inner wall; the dashed lines show strains on the outer wall of the load cell.

Observe that the strain distributions are close to antisymmetric, satisfying

$$\varepsilon_{ij}(\phi) \approx -\varepsilon_{ij}(\phi + 180^\circ)$$

There is a small deviation from perfect antisymmetry. This is due to contact between the load cell and its casing, as discussed below.

Note that our simulations predict that, under transverse loading, the inner section of the load cell will contact the casing. The area of contact at a transverse load of 15000lb is shown as a blue—green region (indicating compressive radial contact stress) in Fig. 10.

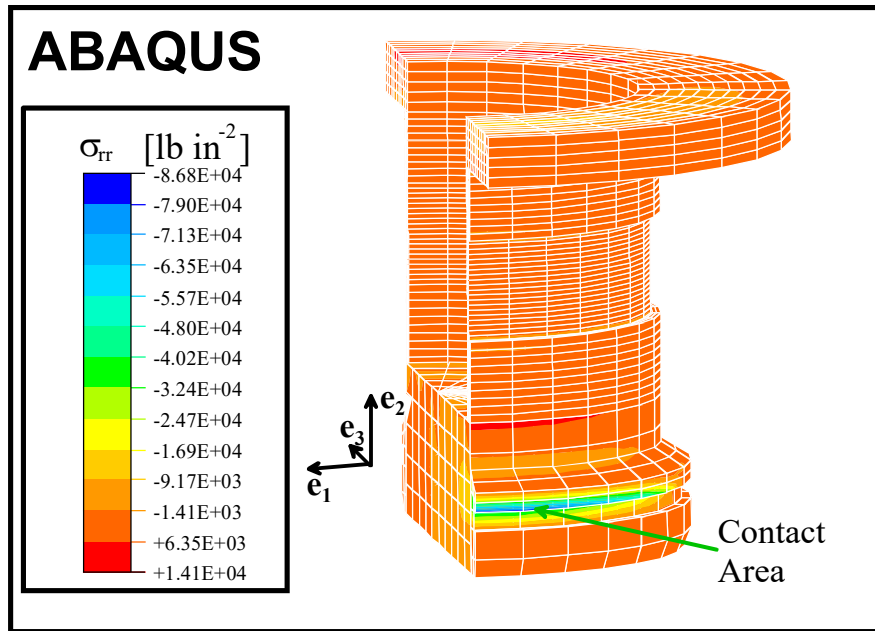


Fig.10: Contours of radial stress in the load cell; illustrating the area of contact between the load cell and the outer casing.

This contact causes a nonlinear relationship between strain and applied force under transverse loading. To determine the extent of this nonlinearity, we have plotted the variation of the maximum value of each strain component with load in Fig. 11. (The maximum value of ε_{zz} occurs at $\phi = -90^\circ$; the maximum value of $\varepsilon_{\theta\theta}$ occurs at $\phi = +90^\circ$ while the maximum value of $\varepsilon_{z\theta}$ occurs at $\phi = 0$). We observe significantly nonlinear behavior, particularly in the shear strain component $\varepsilon_{z\theta}$.

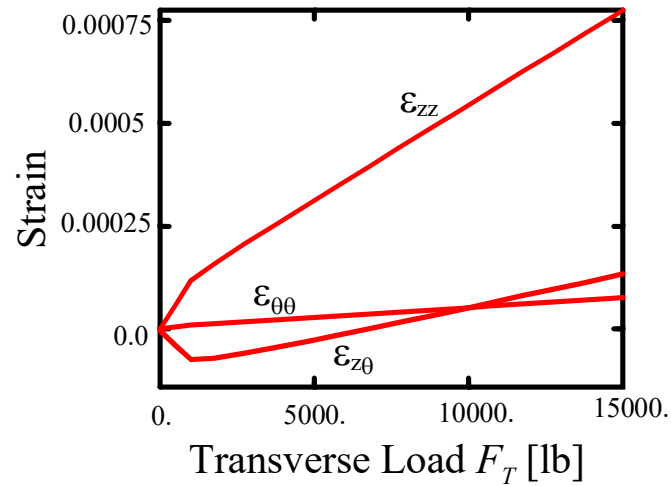


Fig. 11: Variation of maximum strain components in the load cell with transverse load. The strain is not directly proportional to load, due to contact.

2.4 Loading by transverse moment

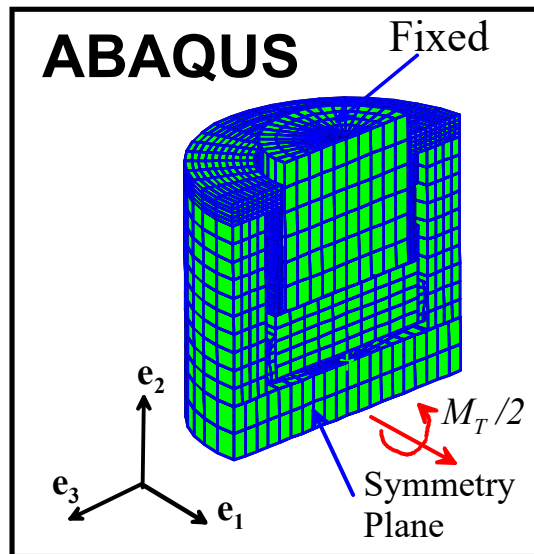


Fig. 12: Mesh and boundary conditions used to compute strains induced in the load cell by transverse moment.

Finally, Fig. 13 shows contours of axial strain ϵ_{zz} , hoop strain $\epsilon_{\theta\theta}$ and shear strain $\epsilon_{z\theta}$ induced in the gage section of the load cell by a unit transverse moment applied to the base, as shown.

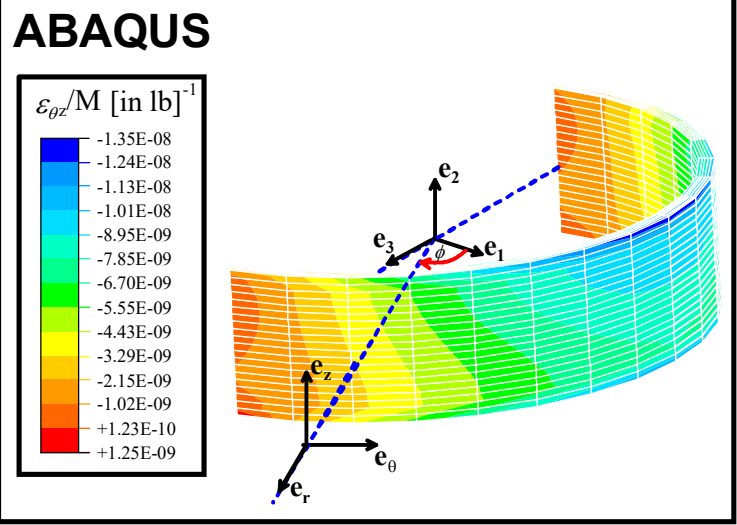
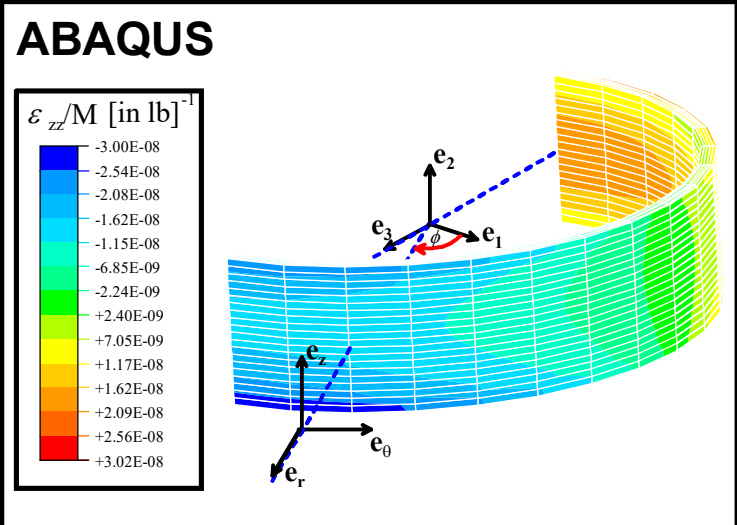
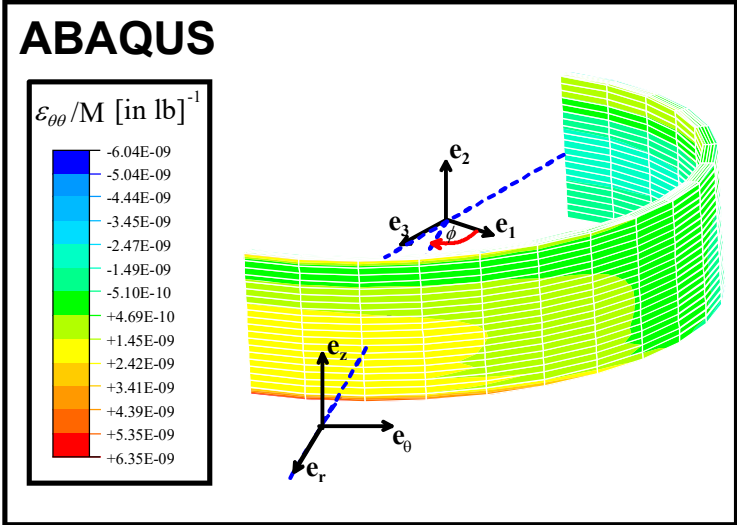


Fig. 13: Contours of strain induced in the gage section of the load cell by transverse moment.

The circumferential variation of each strain component at the midpoint of the gage section is plotted in Fig. 14. Results are shown for both the inner and outer wall of the gage section.

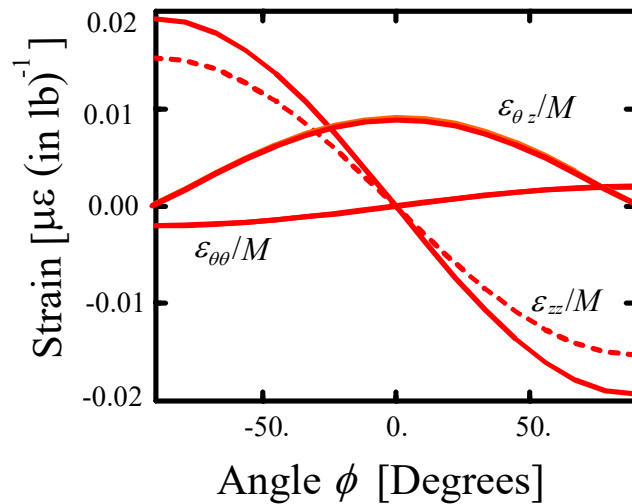


Fig. 14: Circumferential variation of strains at the midpoint of the gage section of the load cell, due to transverse moment loading. The solid lines show strains on the inner wall of the gage section; the dashed lines show strains on the outer wall.

Observe that the strain distributions are close to antisymmetric, satisfying

$$\varepsilon_{ij}(\phi) \approx -\varepsilon_{ij}(\phi + 180^\circ)$$

There is a small deviation from perfect antisymmetry. This is due to contact between the load cell and its casing, as discussed below.

Note that our simulations predict that, under moment loading, the inner section of the load cell will contact the casing. The area of contact is shown as a blue--green region (indicating compressive radial stress) in Fig. 15.

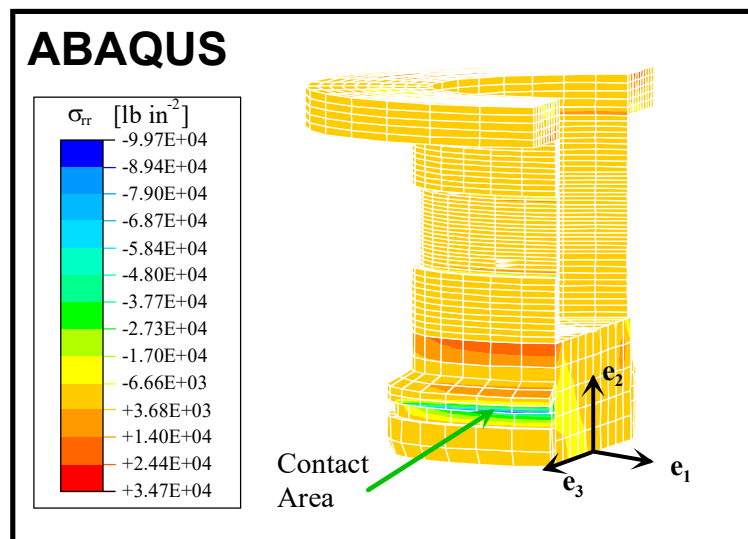


Fig.15: Contours of radial stress in the inner section of the load cell, used to indicate region of contact between the load cell and its casing under transverse moment loading.

This contact causes a nonlinear relationship between strain and applied force under transverse loading. To determine the extent of this nonlinearity, we have plotted the variation of maximum strain with load in Fig. 16 (the maximum value of ε_{zz} occurs at $\phi = 90$; the maximum value of $\varepsilon_{\theta\theta}$ occurs at $\phi = -90$, while the maximum value of $\varepsilon_{z\theta}$ occurs at $\phi = 0$). The applied moment was increased to a value slightly exceeding the specified worst case loading.

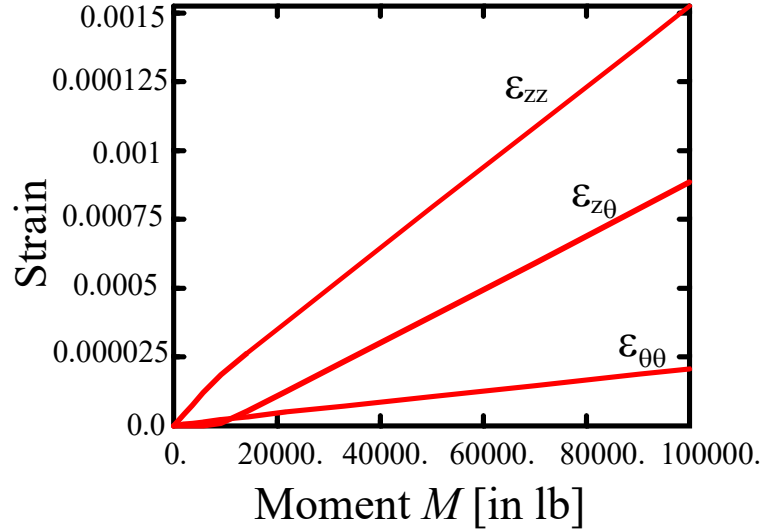


Fig. 16: Variation of maximum strain components induced by transverse moment loading. Strains are not directly proportional to moment, due to contact.

4. Load Cell Calibration.

We note that the strain distributions induced by transverse loading (Sect 3.3) and transverse moment (Sect 3.4) are close to antisymmetric, while the strains induced by axial loading (Sect 3.1) and torsional loading (Sect 3.2) are fully axisymmetric. Consequently, it is possible to largely eliminate the influence of transverse force and transverse bending by averaging readings from two sets of diametrically opposed strain gages.

Assuming that the gages are mounted so as to measure strain at the mid section of the load cell, we predict, for the inner wall of the load cell,

$$\begin{aligned}\bar{\varepsilon}_{zz} &= \frac{1}{2}(\varepsilon_{zz}(\phi) + \varepsilon_{zz}(\phi + 180^\circ)) = 2.81 \times 10^{-8} F_A \\ \bar{\varepsilon}_{\theta\theta} &= \frac{1}{2}(\varepsilon_{\theta\theta}(\phi) + \varepsilon_{\theta\theta}(\phi + 180^\circ)) = -2.34 \times 10^{-8} F_A \\ \bar{\varepsilon}_{z\theta} &= \frac{1}{2}(\varepsilon_{z\theta}(\phi) + \varepsilon_{z\theta}(\phi + 180^\circ)) = 1.61 \times 10^{-8} F_T R\end{aligned}$$

For the outer wall of the load cell, we predict

$$\bar{\varepsilon}_{zz} = \frac{1}{2}(\varepsilon_{zz}(\phi) + \varepsilon_{zz}(\phi + 180^\circ)) = 2.03 \times 10^{-8} F_A$$

$$\bar{\varepsilon}_{\theta\theta} = \frac{1}{2}(\varepsilon_{\theta\theta}(\phi) + \varepsilon_{\theta\theta}(\phi + 180^\circ)) = -2.62 \times 10^{-8} F_A$$

$$\bar{\varepsilon}_{z\theta} = \frac{1}{2}(\varepsilon_{z\theta}(\phi) + \varepsilon_{z\theta}(\phi + 180^\circ)) = 1.61 \times 10^{-8} F_T R$$

Here, forces F_A , F_T are taken to be in lb and the distance of the tool from the symmetry axis R in inches.

The contact between the inner and outer section of the load cell causes a small error in these expressions. Our computations suggest that the expressions for axial and hoop strain are accurate to within $\pm 5\%$; while the expression for shear strain is accurate to within $\pm 0.5\%$. The error increases with the magnitude of transverse force and transverse moment acting on the load cell.

To check the accuracy of the calibration factors, we have computed the strain distribution induced in the load cell by the worst case loading specified by TerraTek. The worst case loading consists of an axial load of 15000lb and transverse load of 12110lb, applied $h = 6$ in below the load cell base and $R = 4.155$ in off axis. The loading was applied as a statically equivalent system of forces and moments acting on the axis of symmetry. We included the effects of friction between the inner section of the load cell and the casing in this computation. Friction was assumed to obey Amonton's law with a coefficient of friction $\mu = 0.1$.

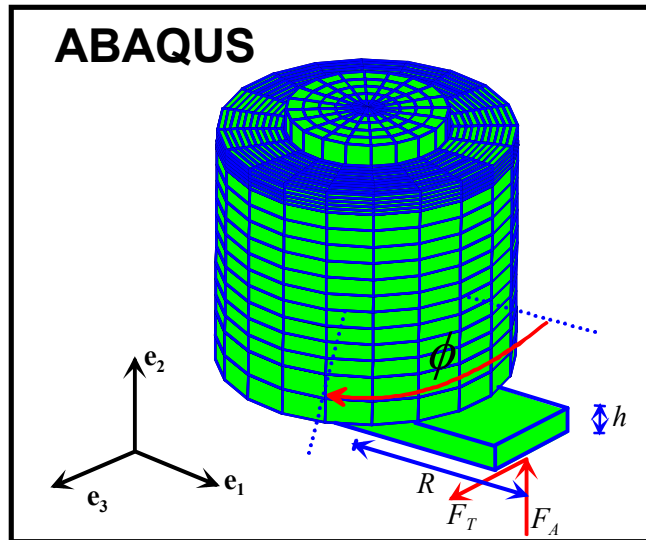


Fig. 17: Notation and sign convention used for calibration test.

Predicted strain distributions on the inner wall of the gage section of the load cell are shown in Fig. 18. The angle ϕ is defined in Fig. 17.

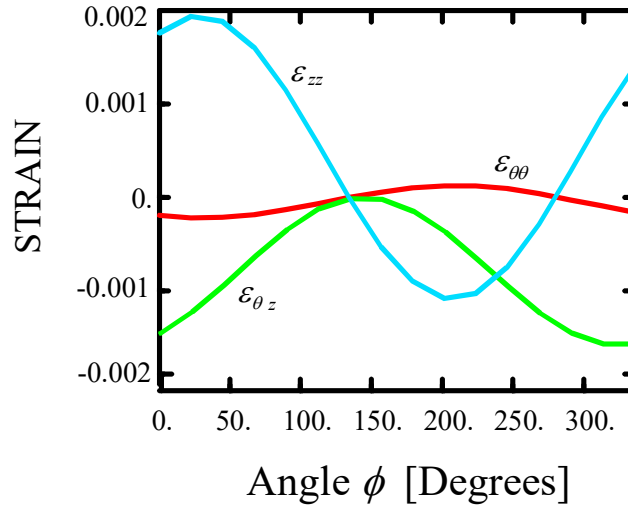


Fig. 18: Strain distribution in the load cell gage section induced by worst case loading

Averaged strain values on the inner wall of the gage section of the load cell were computed to be

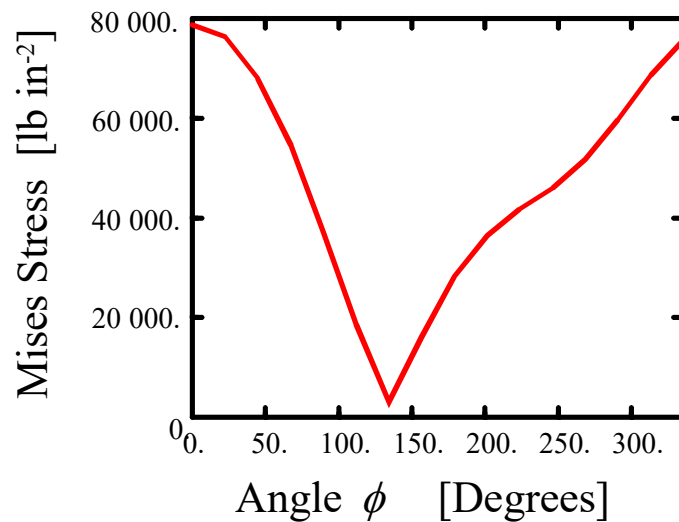
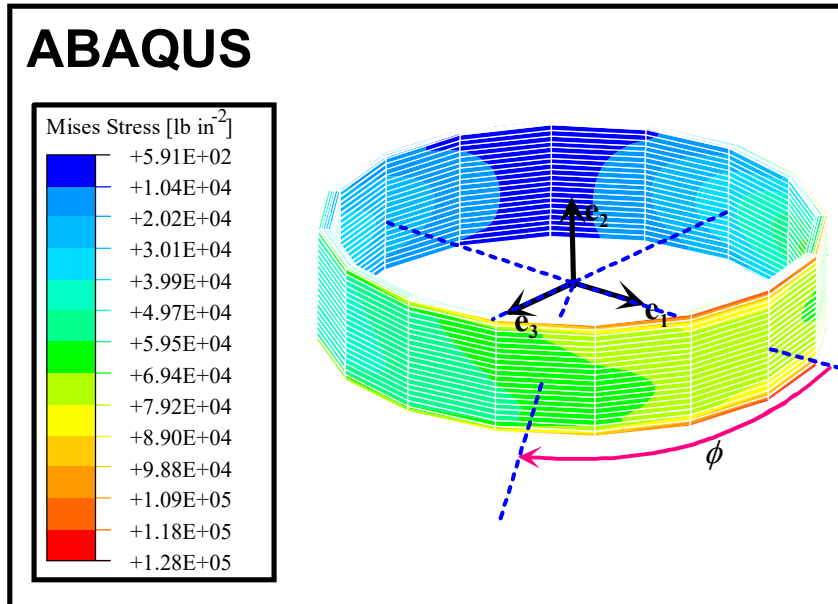
$$\begin{aligned}\bar{\varepsilon}_{zz} &= \frac{1}{2}(\varepsilon_{zz}(\phi) + \varepsilon_{zz}(\phi + 180^\circ)) = 4.32 \times 10^{-4} \pm 0.1 \times 10^{-4} \\ \bar{\varepsilon}_{\theta\theta} &= \frac{1}{2}(\varepsilon_{\theta\theta}(\phi) + \varepsilon_{\theta\theta}(\phi + 180^\circ)) = -4.28 \times 10^{-5} \pm 0.4 \times 10^{-5} \\ \bar{\varepsilon}_{z\theta} &= \frac{1}{2}(\varepsilon_{z\theta}(\phi) + \varepsilon_{z\theta}(\phi + 180^\circ)) = 8.15 \times 10^{-4} \pm 0.05 \times 10^{-4}\end{aligned}$$

These values are within 5% of the values obtained using the calibration factors listed above. It appears that friction will not significantly influence the load cell behavior.

5. Safety Factor.

We have computed the distribution of Mises stress in the gage section of the load cell at maximum load. The boundary conditions for this computation were identical to those used for the calibration check described in the preceding section.

Fig.19 shows contours of Mises stress in the load cell gage section. Fig. 20 shows a graph of the variation of Mises stress around the inner wall of the gage section, at mid height.



Taking a yield stress of 105000 psi for AISI 4140 steel suggests a safety factor of approximately 1.3. Some contained plastic deformation may occur in the region of stress concentration caused by the change in wall thickness of the load cell.